nature communications

Article

https://doi.org/10.1038/s41467-026-78230-4

Anthropogenic aerosol reduction contributes to faster flash drought onset in a changing climate

Received: 1 March 2026

Accepted: 15 September 2026

Published online: 06 October 2026

Check for updates

Jia Wei[1,2], Shuo Wang[1,3] ✉, Weiguang Wang[2,4,5], Jason A. Otkin[6], Diego G. Miralles[7] & Amir AghaKouchak[8,9,10]

Flash droughts have emerged as severe hazards, posing growing challenges to natural and socioeconomic systems, yet the influence of recent aerosol reductions on their onset remains unclear. Here, we investigate the impacts of aerosols and their underlying mechanisms using multi-source observations and large-ensemble climate simulations. Lower aerosol levels are increasingly linked to severe soil moisture deficits, with aerosol effects on onset-speed variability intensifying across 69.2% of regions. During the onset stage, air temperature pathways associated with aerosol variability account for a larger fraction of onset-speed variability than pathways linked to atmospheric demand. Aerosols have long acted to dampen flash drought development; however, their reduction, acting within a warming climate, contributes to faster flash drought onset. As aerosol emissions decline in the future, the area at higher risk of flash drought acceleration in aerosol-forced simulations is projected to increase by 11.7% during 2070–2099 relative to the historical period of 1990–2019.

Flash drought, generally defined as a rapidly developing drought event characterized by an unusually quick onset and intensification over a period of weeks rather than months, has emerged as one of the most devastating hazards in recent decades[1–5]. Observational records indicate that flash drought has become more common, posing severe challenges to agricultural productivity, water security, ecosystem resilience, and socioeconomic stability[6–8]. The exceptionally rapid onset of flash drought causes major challenges for conventional drought monitoring and early warning frameworks, thereby exacerbating socioeconomic and ecological impacts[9,10]. Various mechanisms, such as persistent atmospheric ridges, Rossby wave trains emanating from remote forcing, and changes in land–atmosphere feedbacks, have been shown to lead to flash drought onset[1,11]. While research has indicated that greenhouse gases can lead to more flash droughts[8], anthropogenic aerosols and their interplay with land–atmosphere processes during the onset of flash droughts remain poorly understood. With the implementation of global pollution control measures, anthropogenic aerosol concentrations have markedly declined over recent decades[12–14]. This reduction may increase the local warming rate and accelerate the rapid decline of soil moisture by increasing atmospheric water demand and intensifying land–atmosphere feedbacks. Ultimately, onset speed is a function of the balance between soil

[1]State Key Laboratory of Climate Resilience for Coastal Cities, Department of Land Surveying and Geospatial Science, The Hong Kong Polytechnic University, Hong Kong, China. [2]College of Hydrology and Water Resources, Hohai University, Nanjing, China. [3]Otto Poon Research Institute for Climate-Resilient Infrastructure and Research Institute for Land and Space, The Hong Kong Polytechnic University, Hong Kong, China. [4]Yangtze Institute for Conservation and Development, Hohai University, Nanjing, China. [5]National Key Laboratory of Water Disaster Prevention, Hohai University, Nanjing, China. [6]Cooperative Institute of Meteorological Satellite Studies, Space Science and Engineering Center, University of Wisconsin–Madison, Madison, WI, USA. [7]Hydro-Climate Extremes Lab (H-CEL), Ghent University, Ghent, Belgium. [8]Department of Civil and Environmental Engineering, University of California, Irvine, CA, USA. [9]Department of Earth System Science, University of California, Irvine, CA, USA. [10]United Nations University Institute for Water, Environment and Health, Richmond Hill, ON, Canada. ✉e-mail: shuo.s.wang@polyu.edu.hk

moisture declines and evaporation increases, with both being affected by aerosols in complex ways[15,16].

Quantifying the influence of aerosols on flash drought development is challenging due to complex multi-scale interactions in aerosol–cloud–radiation processes[17,18], and their effects on the ultimate drivers of soil dry-out[1,19]. This complexity is especially pronounced during the onset stage, when rapid shifts in soil moisture and evaporative demand occur over short timescales, making aerosol-related impacts difficult to isolate from internal weather variability. The difficulty is compounded by the strong spatiotemporal heterogeneity of anthropogenic aerosols and their nonlinear effects on hydrometeorological processes[20–22]. Understanding aerosol–flash drought interactions has become increasingly urgent as climate mitigation efforts have reduced anthropogenic aerosol concentrations, potentially altering cloud cover and increasing atmospheric water demand, thereby affecting soil dry-out[13,23]. Existing aerosol–drought studies have predominantly focused on the impacts of aerosols on the trend of long-term drought[14,24]; however, the mechanisms underlying the rapid onset of flash droughts over short timescales, and particularly the contributions of aerosols to their development processes, remain poorly understood. Hence, in-depth studies on how aerosol changes influence the accelerated soil moisture deficits within subseasonal timescales are imperative and motivate our present research.

Here, we investigate the changing behavior of aerosols during the onset stage of flash droughts using multiple datasets, including aerosol optical depth (AOD) observations from the Moderate Resolution Imaging Spectroradiometer (MODIS[25]) and AERONET[26,27] for the period 2003–2024. Soil moisture is obtained from the daily European Space Agency Climate Change Initiative (ESA CCI) dataset[28]. We analyze the spatiotemporal variations in onset speed and AOD during flash drought onset and investigate their relationship using copula methods. We subsequently explore the non-stationary impact of aerosols on flash drought onset speed using a Bayesian dynamic linear model (DLM) and further quantify this impact using large ensemble climate model simulations from the Coupled Model Intercomparison Project Phase 6 (CMIP6[29,30]). To elucidate physical mechanisms, we construct pathway networks to examine the influence of aerosols on climatic conditions and their radiative effects during flash drought onset. This understanding is crucial for clarifying the role of aerosols in modulating flash drought development. Finally, we project changes in flash drought onset speed using simulations driven by anthropogenic aerosols, providing deeper insights into regional risks of accelerated flash drought development under future aerosol reductions. Our findings have important implications for improving flash drought predictability and for formulating effective regional adaptation strategies under climate mitigation.

Results

Global evolution of flash drought onset speed and aerosol optical depth

Subseasonal drought has increasingly transitioned toward flash drought, characterized by a rapid decline in soil moisture driven by intensified atmospheric water demand, making flash drought a new normal among extreme climate events[1,31]. Understanding potential future variations in flash drought onset speed is critical for early warning systems and drought preparedness strategies[9], highlighting the need for a comprehensive analysis of how onset speeds vary across time. We first analyzed flash drought onset speed based on soil moisture from the ESA CCI dataset (Fig. 1a). To enable direct comparison between aerosol variability and flash drought onset speed, both variables were converted to standardized series. For analyses at regional and global scales, AOD values were first spatially averaged using area weights before standardization. We hereafter refer to this standardized index as AOD_z to distinguish it from raw aerosol optical depth. Results show spatial heterogeneity with relatively high onset speeds occurring across broad regions of North America, Asia and parts of South America and Africa. In recent years, standardized flash drought onset speed has exhibited consistent acceleration across all IPCC SREX regions (Fig. 1b and Supplementary Table S1). These results suggest an accelerated onset of flash drought, reflecting intensified regional responses to changing climatic conditions.

During flash drought onset, AOD_z also exhibits distinct temporal changes, decreasing significantly from 2003 to 2024. The time series of AOD_z during the onset stage shows a notable divergence from the significant acceleration in flash drought onset speed (Fig. 1c). These results indicate that aerosols have decreased significantly during flash drought development in recent decades. The divergence between AOD evolution and onset speed reveals distinct changes, suggesting more complex interactions between atmospheric aerosol loading and flash drought intensification processes. Consequently, the role of aerosols during flash drought outbreaks and their changing relationship with drought intensification mechanisms require further detailed investigation.

Dynamic relationship between aerosol and onset speed during flash drought onset

We first investigated the concurrence of aerosol loading and soil moisture decline for each pentad (current minus previous). The spatial pattern of bivariate dependence reveals an extensive distribution of concurrent low aerosol (below the 30th percentile) and soil moisture decline (below the 30th percentile), with higher probabilities across most of the global land (Fig. 2a). This result suggests that aerosol–soil moisture decline exhibits strong dependency, which may be driven by conditions favoring flash drought development through aerosol-induced climatic effects and local land–atmosphere feedback mechanisms[32–34]. We further examined the relationship between lower aerosol levels and soil moisture declines across multiple severity thresholds. The relationships between lower aerosol levels and various soil moisture extremes are quantified using the probability multiplication factor (PMF). Regional PMF results indicate a stronger coupling of lower AOD (below the 30th percentile) with extreme soil moisture decline (below the 5th percentile) than with moderate soil moisture decline (below the 30th percentile) (Fig. 2b). The concurrence of lower aerosol levels with five severities of soil moisture decline (at the 40th, 30th, 20th, 10th, and 5th percentiles) was also analyzed. PMF values increase as the soil moisture deficits become more severe, ranging from the 40th percentile to the most extreme 5th percentile (Supplementary Fig. 1). These results indicate that the co-occurrence of diminished aerosol concentrations and soil moisture depletion intensifies as moisture deficits become more severe. These findings suggest that a reduction in atmospheric aerosols may enhance the probability of rapid soil moisture decline. Thus, we further investigate the impacts of aerosols on flash drought onset speed.

We employed a Bayesian dynamic linear model (DLM) using detrended AOD and climatic factors affecting flash drought onset speed as predictors and detrended flash drought onset speed as the predictand. We first removed linear trends from AOD, flash drought onset speed, and the associated climatic variables to minimize associations arising from shared long-term changes and to focus the DLM analysis on the time-varying relationship between aerosol variability and flash drought onset speed. The detrended climatic factors, including surface temperature, shortwave radiation, precipitation, vapor pressure deficit, soil moisture, vertically integrated moisture divergence and 850 hPa vertical velocity, were first selected using the variance inflation factor (VIF) and then used as predictors. Meanwhile, we removed these confounding effects on AOD to isolate aerosol signals before DLM simulation. The Bayesian DLM provides the time-varying impacts of the predictors on the predictand within the examined period[35,36], enabling investigation of the non-stationary effects of

https://doi.org/10.1038/s41467-026-78230-4

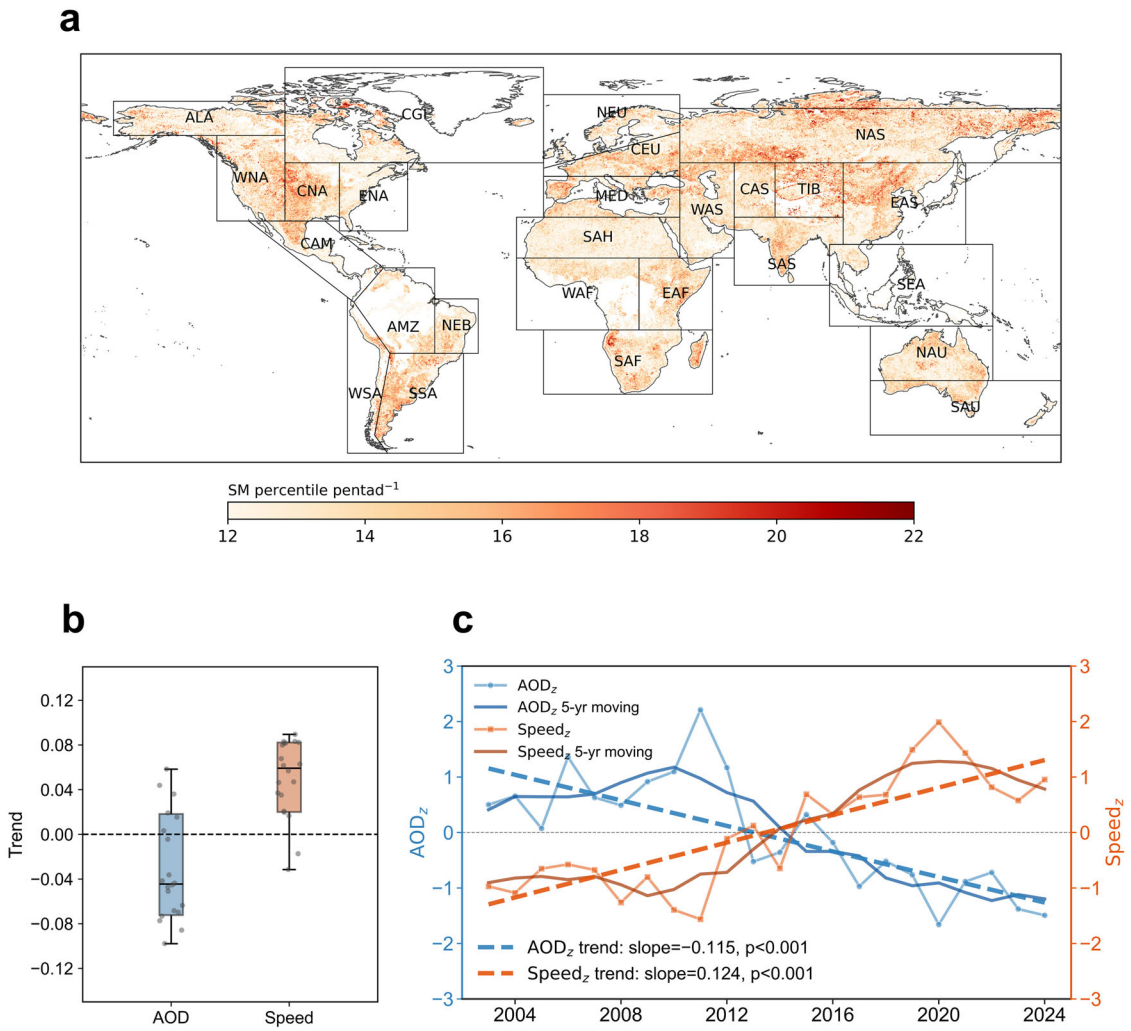


Fig. 1 | Global evolution of onset speed and aerosol optical depth (AOD) during the flash drought onset stage. a Spatial distribution of flash drought onset speed (soil moisture percentile pentad^{-1}) for 2003–2024. **b** Trends in standardized AOD (AOD$_z$) and onset speed (Speed$_z$) for each IPCC SREX region. The onset speed of flash drought was calculated at the grid level and then averaged over the IPCC regions weighted by area. The boxes contain 25–75th percentiles, and the whiskers indicate the 5th–95th percentiles. **c** Interannual variability of the global standardized time series of Speed$_z$ and AOD$_z$ during the flash drought onset stage. The 5-year moving average time series and linear trends for Speed$_z$ and AOD$_z$ are indicated with thick solid and dashed lines, respectively. The significance level for each trend is indicated at the bottom of the panel.

aerosols on flash drought onset speed. Results show that Bayesian DLM simulations captured both the magnitude and interannual variability of the observed onset speed for each region. The Bayesian DLM simulations account for 63.4–96.7% (STD_{dlm}/STD_{obs}) of the observed onset speed variability across different regions (Supplementary Fig. 2) and are highly correlated with observed onset speed.

In recent years, the impact of AOD on flash drought onset speed exhibited an increasing tendency in the regions shown in Fig. 2c, which account for 69.2% of all regions. The variance in onset speed explained by AOD increased significantly in 18 regions (Supplementary Fig. 3). In these regions, the average explained variance of aerosols increased from 33.9 to 57.8%. This indicates a strengthening linkage between aerosol variability and onset speed in recent decades. Such temporal evolution and spatial heterogeneity may reflect changes in the radiative and climatic effects of regional aerosol variations, which are influenced by underlying surface characteristics[16,37]. With enhanced coupling and association between aerosols and flash drought acceleration, aerosol changes may have played an increasingly important role in modulating flash drought dynamics in recent decades, with potential implications for regional water security and agricultural resilience.

Physical processes driving the aerosol-induced acceleration of flash drought onset speed

We conducted structural equation modeling to investigate the complex causal pathways through which aerosols may influence flash drought onset speed via atmospheric mechanisms. We performed two separate path analyses: one disentangling the influence of aerosols on surface air temperature, and the other focusing on the radiative effects of aerosols[38–40]. The structural equation model demonstrates robust statistical significance, with high fit indices confirming the validity of the depicted path relationships. Results suggest that higher AOD decreases surface air temperature but is positively associated with cloud cover (Fig. 3a). This agrees with the cooling effect of aerosols and their role as cloud condensation nuclei, which can further facilitate cloud cover development. Notably, air temperature has a significant negative impact on soil moisture, underscoring its critical role in reducing soil water content and thereby accelerating flash drought onset. Meanwhile, cloud cover has a strong negative impact on shortwave radiation, which has an opposite effect on onset speed. Overall, aerosols influence flash drought onset speed through temperature and cloud cover pathways, predominantly by modulating soil moisture and shortwave radiation. For the direct radiative effects of

https://doi.org/10.1038/s41467-026-78230-4

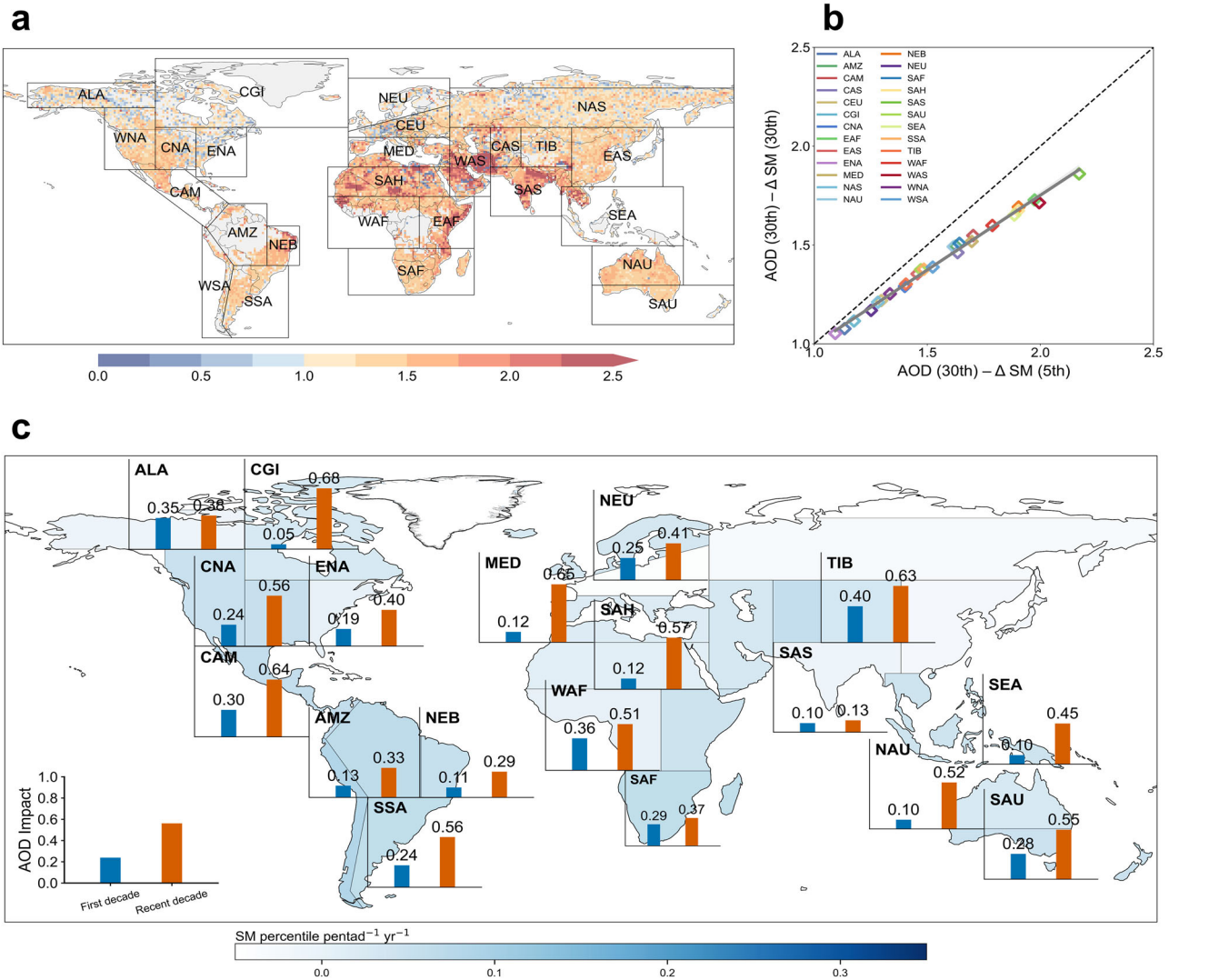


Fig. 2 | Impacts of aerosol on flash drought onset speed. a Probability multiplication factor (PMF) for concurrent low AOD (below the 30th percentile) and extreme soil moisture decline (Δ soil moisture; current pentad minus previous pentad, below the 30th percentile) from 2003 to 2024. A PMF ≤ 1 represents no increase in the joint probability. **b** PMF values for lower AOD and different soil moisture decline levels (below the 30th and 5th percentiles) across the IPCC SREX regions. The bias relationship ($x = 1.32\,y + 0.32$) reflects a stronger coupling between lower AOD and soil moisture decline. The PMF was calculated at the grid level and then averaged over the IPCC regions weighted by area. **c** Impacts of AOD on flash drought onset speed, showing the standard deviation of AOD contributions for the first decade (2003–2012) and the recent decade (2015–2024) in each IPCC SREX region. Blue shaded areas on the global map indicate the trend of flash drought onset speed for each region.

aerosols, we conducted path analyses to demonstrate how aerosols are associated with changes in the surface energy balance and evaporation (Fig. 3b). The negative correlation between aerosols and shortwave radiation reflects the established direct radiative effect, whereby particulate matter attenuates incoming solar radiation through scattering and absorption[15,41]. Shortwave radiation shows a positive correlation with evaporation, which further exacerbates flash drought development.

Based on the influence of aerosols on surface temperature and radiation, we synthesized the essential pathways elucidating how aerosols are statistically linked to variations in flash drought onset speed (Fig. 3c). With aerosol reduction during the onset stage, enhanced surface temperature is associated with decreased soil moisture, exacerbating the acceleration of flash drought onset. Simultaneously, increased shortwave radiation increases evaporation, accelerating soil moisture decline. Ultimately, enhanced evaporation and decreased soil moisture collectively increase onset speed, effectively accelerating flash drought initiation. These results illustrate how aerosols are associated with changes in atmospheric variables and the energy balance during the onset stage. Under conditions of aerosol reduction, both temperature and radiative effects are conducive to reduced soil moisture and enhanced evaporation, thereby contributing to a faster onset speed. Furthermore, we compared the parallel effects of potential evaporation and vapor pressure deficit (Supplementary Fig. 4). The aerosol-induced changes in potential evapotranspiration and vapor pressure deficit are similar during the onset stage of flash drought but are weaker than the aerosol-induced temperature effects.

Historical and future impacts of anthropogenic aerosols on onset speed

Anthropogenic aerosols generally exert a cooling influence, thereby partially masking the full extent of global warming[15,22]. Relative to pre-industrial conditions, human-induced climate forcings have significant impacts on flash drought acceleration. Greenhouse gas forcing leads to a pronounced global acceleration of flash drought onset speed. In

https://doi.org/10.1038/s41467-026-78230-4

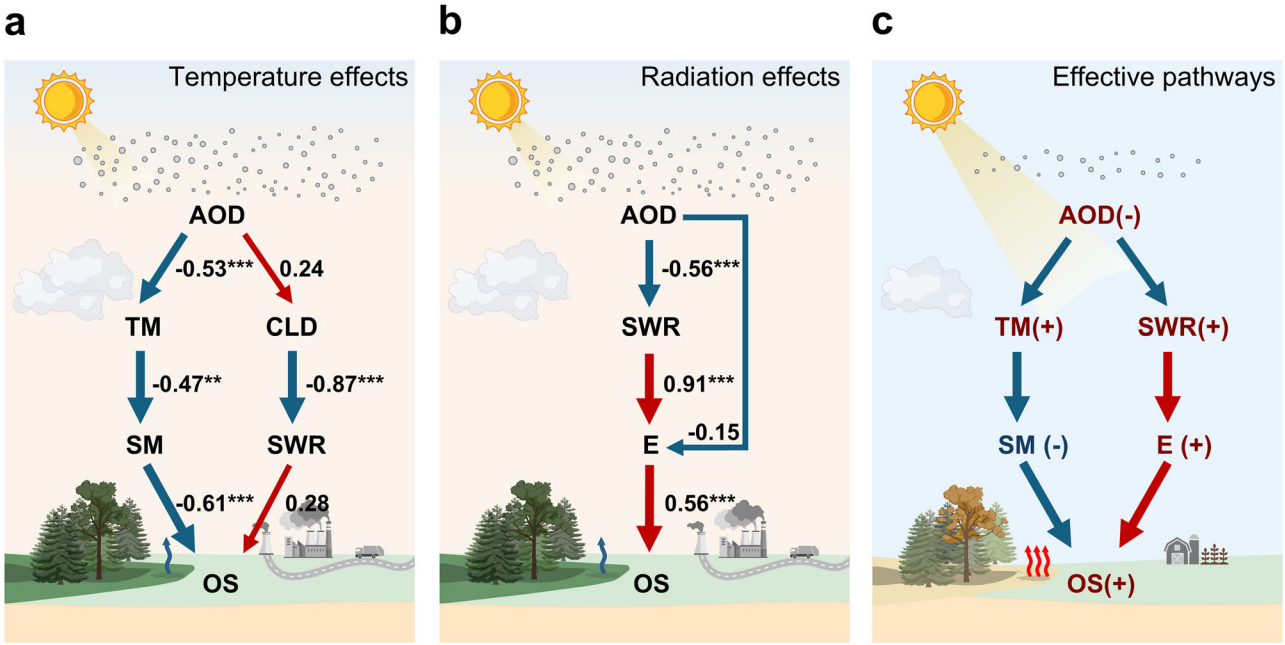


Fig. 3 | Atmospheric pathway networks linking aerosols and flash drought onset speed. a Temperature pathway of aerosols during the flash drought onset stage, including surface air temperature, total cloud cover, shortwave radiation, and soil moisture. **b** Radiative pathways of aerosols during flash drought onset, including shortwave radiation and evaporation. **c** Effective pathways linking aerosol changes to variations in flash drought onset speed. Factor loadings between variables are shown next to the arrows ($P < 0.001$, ***; $P < 0.01$, **; $P < 0.05$, *). The color and width of the arrows indicate the direction (positive or negative) and magnitude of the effect, respectively. The statistical fit indices for the temperature and radiation pathways are as follows: Comparative Fit Index (0.81 and 0.95), Goodness-of-Fit Index (0.76 and 0.91), and Standardized Root Mean Square Residual (0.17 and 0.08). AOD, TM, CLD, SM, SWR, E, and OS represent aerosol optical depth, surface air temperature, total cloud cover, soil moisture, shortwave radiation, evaporation, and flash drought onset speed, respectively.

contrast, with increases in anthropogenic aerosols, flash drought onset shows a widespread slowdown (Supplementary Fig. 5). This highlights the dominant and opposing roles of greenhouse gas warming and anthropogenic aerosol cooling in shaping historical variations in flash drought development. However, with international attention and cooperative solutions targeting emissions, global mitigation efforts have resulted in significant decreases in anthropogenic aerosols. We further explored the risk ratio changes in flash drought acceleration driven by anthropogenic aerosols in recent years (Fig. 4a). The risk ratio quantifies the likelihood of changes in onset speed driven by anthropogenic aerosol-only (AA-only) forcing relative to natural climate forcing, with values greater than 1.0 indicating an increased risk of accelerated flash drought development. Results showed that extensive regions exhibited stronger risks. Globally, the majority of land area (59.9%) experienced anthropogenic aerosol-driven acceleration of flash drought onset. Regionally, higher risks of accelerated flash drought onset associated with anthropogenic aerosol-only forcing were evident in CNA (75.0%), MED (69.3%), and AMZ (62.4%), overlapping with areas showing stronger AOD-related impacts calculated from observation-based results (Fig. 4b). Although anthropogenic aerosols slowed flash drought onset relative to the pre-industrial period (Supplementary Fig. 5b, d), this slowdown effect appeared to be weakening in recent years.

Furthermore, we analyzed the future risk ratio of flash drought onset speed and its trend from 2030 onward. We selected the SSP2-4.5 scenario as the primary future shared socioeconomic pathway, as it represents a moderate emissions condition that reflects the continuation of current global trends with strengthened climate policies. SSP2-4.5 serves as a widely adopted baseline scenario in IPCC AR6 assessments[29]. Additionally, SSP2-4.5 is the only scenario that provides future projections for AA-only forcing experiments under the Detection and Attribution Model Intercomparison Project (DAMIP) framework[30]. Thus, we analyzed projected changes in flash drought onset speed under SSP2-4.5 prior to investigating their responses to different anthropogenic drivers. The projected temporal evolution of global flash drought onset speed under the CMIP6 SSP2-4.5 scenario indicates a consistent acceleration of flash drought (Supplementary Fig. 6). All climate model projections demonstrate statistically significant positive trends, suggesting an acceleration of flash drought development rates throughout the 21st century. With global carbon neutrality commitments targeting mid-century achievement, the transitional period of 2030–2059 represents a critical window during which anthropogenic emissions will continue to drive climate change[42,43].

From 2030 to 2059, onset speed trends show distinct regional patterns, with several regions exhibiting statistically significant increases, implying that flash droughts will develop more rapidly during 2030–2059 (Supplementary Fig. 7). Meanwhile, most regions are projected to experience higher risks of flash drought acceleration under AA-only forcing in 2030–2059 (Fig. 4c) relative to natural-only forcing. This heterogeneous spatial distribution reflects the combined influence of anthropogenic aerosols and regional climate responses in CMIP6 simulations. In the late 21st century (2070–2099), future increases in flash drought onset speed trends under anthropogenic aerosol forcing scenarios are projected to be more extensively distributed (Supplementary Fig. 8). Meanwhile, higher risk ratios continue to occur in most regions (Fig. 4c). Larger areas are projected to experience higher risk than in the mid-century period (Supplementary Fig. 9). With the future decline in anthropogenic aerosol in model simulations (Supplementary Fig. 10), risks are projected to show a persistent increase within anthropogenic aerosol-forced simulations. Consequently, as the damping effect of anthropogenic aerosol weakens in the future, flash drought acceleration is projected to intensify. These findings underscore the importance of long-term monitoring, especially in regions exhibiting consistent positive trends, where faster

https://doi.org/10.1038/s41467-026-78230-4

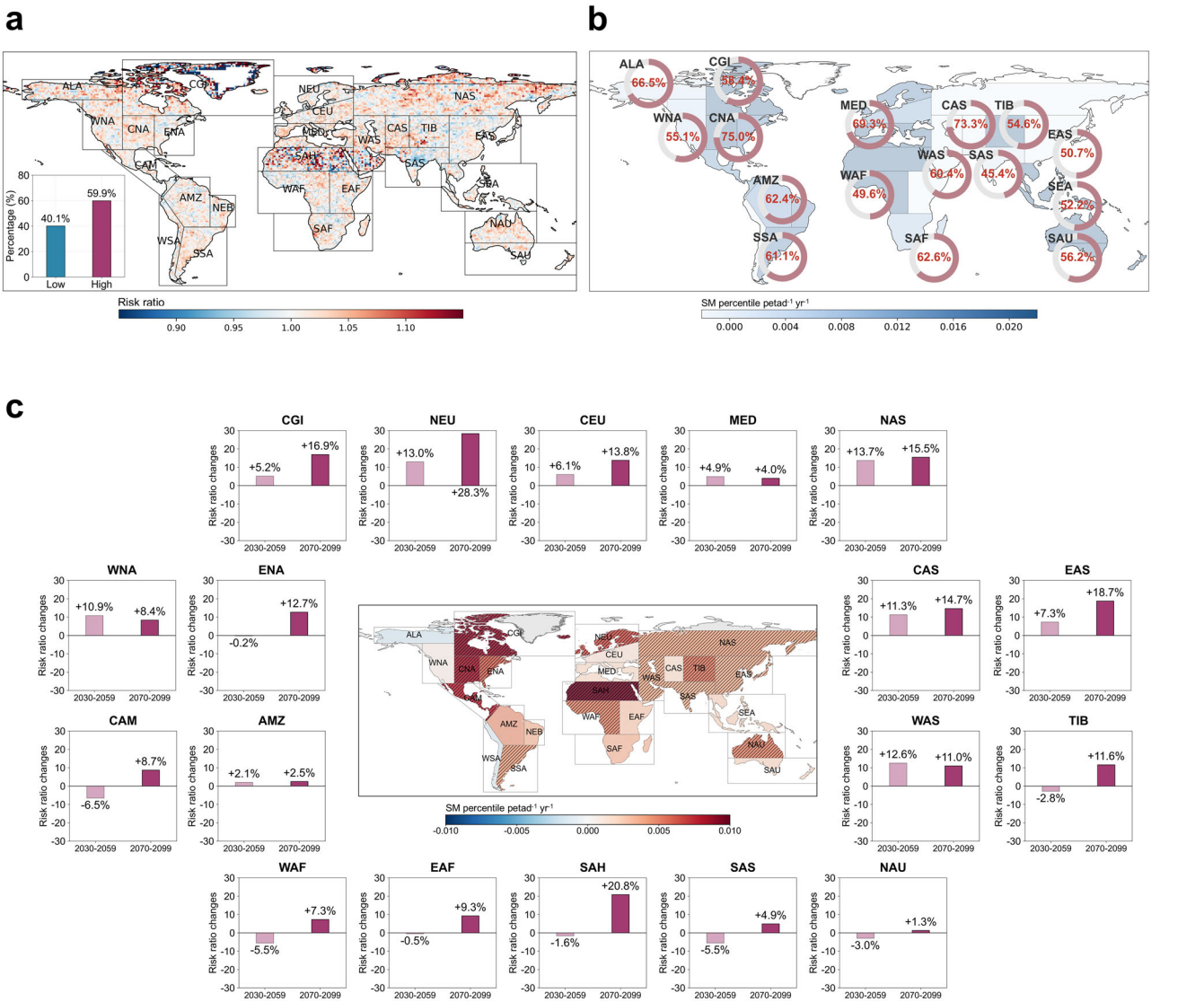


Fig. 4 | Risk of flash drought acceleration under anthropogenic aerosols-only (AA-only) forcing. a Risk ratio of flash drought onset speed from AA-only forced CMIP6 model simulations at each grid cell for 1990–2019. Values above 1 indicate a higher risk of accelerated flash drought onset. **b** Regional risk of accelerated flash drought onset driven by AA-only forcing. Blue shaded areas on the global map indicate the trend of aerosol impacts on flash drought onset speed in each region based on historical observations. **c** Future changes in the risk of accelerated flash drought onset driven by AA-only forcing for 2030–2059 and 2070–2099 relative to 1990–2019. The spatial pattern shows the trend of onset speed driven by AA-only forcing for 2030–2099. Significant trends are indicated with black hatched lines.

onset speeds can reduce preparedness time and increase the vulnerability of exposed populations and ecosystems.

Discussion

The observed AOD evolution shows consistent temporal behavior across independent datasets. In our study, the comparison between MODIS and AERONET shows consistent AOD magnitude, interannual variability, and long-term changes (Supplementary Fig. 11), suggesting the robustness of AOD variability during flash drought onset under observed conditions. This is also consistent with long-term evaluations demonstrating good temporal stability of MODIS Collection 6.1 relative to AERONET[44]. However, changes in cloud occurrence may alter sampling density and introduce uncertainty into AOD variability. Because AERONET direct-sun observations are cloud-screened, this comparison cannot fully constrain aerosol variations missed during cloudy conditions. Previous studies have shown that such sampling effects are generally limited for globally aggregated AOD statistics but can influence sampling representativeness, depending on spatial scale and cloud conditions[45,46]. Therefore, although the consistency between MODIS and AERONET supports the robustness of the observed AOD variability under available clear-sky conditions, the influence of this sampling limitation on AOD variability remains uncertain in persistently cloudy environments. For model simulations, we assessed 11–37 ensemble members from each CMIP6 climate experiment (Supplementary Table 2), using available models that provide daily surface soil moisture outputs. Comparisons between observational results and CMIP6 historical simulations reveal spatial consistency in flash drought characteristics (Supplementary Fig. 12). Furthermore, these flash drought characteristics exhibit agreement across different models, reflecting reliable representations of soil moisture dynamics in the land surface components currently coupled within climate modeling systems[47–54]. Consistent hotspot regions (e.g., North America, southern Africa, and central Asia) are captured by both observations and models, except for Greenland and the Sahara, where soil moisture conditions are extreme[55,56]. Overall, the strong spatial correspondence between observations and CMIP6 simulations strengthens confidence in using these climate models to investigate flash drought characteristics. Besides model validation, we performed

a sensitivity analysis to test whether the identified flash droughts depend on the soil moisture decline thresholds. Across a range of onset speed thresholds (5–20% per pentad), the spatial distributions of flash droughts exhibit a globally similar pattern (Supplementary Fig. 13). The hotspot regions of rapid flash drought remain consistent when using different thresholds, indicating that the choice of onset speed threshold does not fundamentally alter conclusions regarding regional flash drought evolution.

Comparing the observation-based and model-based results helps to better understand the regional heterogeneity in the influence of aerosol on flash drought onset speed. The observed AOD is a bulk-column optical measure that reflects total aerosol loading from both anthropogenic and natural sources, including mineral dust, sea salt, biomass-burning smoke, and aerosols transported over long distances, rather than anthropogenic aerosol loading alone. Accordingly, we complement the observational aerosol results with AA-only experiments, in which anthropogenic aerosol forcing is prescribed separately from other external forcings, to provide an independent constraint on the anthropogenic aerosol contribution. By comparing observed and modeled results (Fig. 4b), we found that high risks of flash drought acceleration under AA-only forcing generally overlap with stronger observation-based AOD impacts. However, discrepancies occur in South Asia, the Tibetan Plateau, Southeast Asia, and several arid regions. Such discrepancies may partly reflect regional differences in aerosol source composition and transport pathways, including long-range transport of black carbon to the Himalayas and Tibetan Plateau[57,58], mineral dust transported to the Tibetan Plateau from multiple desert source regions[59], transboundary biomass-burning emissions in Southeast Asia[60], and substantial contributions from natural dust sources in arid regions[61]. Because observed AOD reflects the combined effects of anthropogenic and natural aerosols, the regional agreement should be interpreted as consistency rather than a direct validation of the anthropogenic aerosol contribution. Beyond differences in sources and transport, land–atmosphere interactions may further contribute to regional differences between observation-based and AA-only simulations. Biomass-burning smoke can interact strongly with clouds, the planetary boundary layer, and regional circulation. Over Southeast Asia, biomass-burning aerosols have been shown to enhance low cloud formation through coupled aerosol–cloud–boundary layer interactions and modulate monsoon circulation[62]. Similar associations between smoke aerosols and low clouds have also been reported over the Indian region[63]. These processes suggest that observed AOD-based relationships may incorporate effects of biomass burning, aerosol transport, and meteorological feedbacks that are not directly comparable to the response isolated in prescribed AA-only experiments.

Future projections show large spatial heterogeneity in the risk of flash drought acceleration driven by AA-only forcing. Among the regions projected to experience accelerated flash drought, some instead show weakened contributions from anthropogenic aerosols in 2030–2059. The rapid aerosol reductions before mid-century could induce pronounced increases in surface temperature and shortwave radiation, whereas the incremental radiative and thermal effects of further aerosol removal weaken once loading has already declined to a low level[14]. In moisture-limited regions, the additional shortwave radiation is increasingly partitioned into sensible rather than latent heat, which limits increases in evaporation and soil moisture depletion[64,65]. By the late 21st century, most regions are projected to experience more rapid AA-only driven flash drought, except for some arid regions such as WAS. The projected weakening of aerosol is largely governed by large-scale circulation change, particularly a weakening of the northwesterly dust transport pathway, accompanied by locally reduced surface wind speed, reducing the aerosol-attributed acceleration of flash drought[66]. Future hydroclimatic responses to aerosol forcing may vary regionally due to differences in climate conditions[67,68]. These nonlinear forcing responses, land-surface constraints, and circulation changes affect the localized anthropogenic aerosol-related flash drought risk. Thus, more in-depth research on aerosol and extreme event interactions in these regions is needed to better understand hydroclimatic risks modulated by complex aerosol sources, rapid emission changes, and strong land–atmosphere feedbacks.

In this study, we integrated multi-source observational datasets, products and large-ensemble CMIP6 simulations to examine the influence of aerosols on flash drought acceleration and to quantify changes in onset speed driven by anthropogenic aerosols. Atmospheric aerosols have emerged as a critical modulator of flash drought dynamics, playing an increasingly important role in recent years. Our analyses reveal a strengthening statistical association between onset speed and aerosol variability during flash drought development. The AA-only forcing model experiments show that anthropogenic aerosols during the industrial period have masked flash drought acceleration; however, the risk of acceleration relative to natural forcing conditions has intensified in recent decades with the reduction of anthropogenic aerosols. The mechanisms through which aerosols affect flash drought onset are multifaceted. The dominant pathway is the increase in surface air temperature and shortwave radiation associated with aerosol variability during the onset stage, contributing to greater evaporation and soil moisture depletion where moisture availability permits. The identification of distinct mechanistic pathways linking aerosols to flash drought onset has significant implications for understanding the physical processes influencing flash drought evolution.

Future projections indicate accelerated flash drought in both the 2030–2059 and 2070–2099 periods. Under the SSP2-4.5 scenario, strengthened air-quality and emission-control policies are expected to cause a substantial decline in aerosol emissions in future decades. Such policy-driven reductions, while yielding major co-benefits for public health and atmospheric clarity, may be associated with faster flash drought onset. For the AA-only experiments, future projections point to regionally heterogeneous flash drought acceleration, as well as higher risks that become more pronounced from mid-century (2030–2059) to late-century (2070–2099). The higher risk of this acceleration poses substantial challenges for ecosystem resilience and agricultural productivity, emphasizing the need for improved early warning systems and adaptive management strategies. Future regional vulnerability patterns provide a critical scientific foundation for targeted mitigation and for advancing subseasonal-to-seasonal drought prediction[2]. Our results highlight the imperative need for integrated assessment approaches that consider the combined influence of anthropogenic aerosols and other human-induced impacts in shaping future hydroclimatic extremes.

Methods

Observations

Daily AOD was obtained from the Moderate Resolution Imaging Spectroradiometer (MODIS) Collection 6.1 Level 3 global data (i.e., MOD08_D3 from Terra and MYD08_D3 from Aqua)[25]. The MODIS AOD retrievals use the Dark Target and Deep Blue algorithms, enabling the characterization of spatiotemporal variations in atmospheric aerosol loading[44,69,70]. The Terra MODIS record begins in February 2000, whereas the Aqua MODIS record begins in July 2002. Ground-based AOD observations were obtained from Version 3 Level 2.0 of the Aerosol Robotic Network (AERONET), a globally distributed network of calibrated sun-sky radiometers providing quality-assured measurements of spectral columnar aerosol loading[26,27]. AERONET measurements were temporally collocated with the MODIS retrievals and spatially matched to the corresponding MODIS grid cells to independently evaluate the AOD variations identified from the satellite retrievals during flash drought onset (Supplementary Fig. 11). The study was

restricted to the period of overlapping Terra and Aqua MODIS coverage to ensure the availability of observations from both satellites.

Daily surface soil moisture was obtained from Version 09.2 of the European Space Agency Climate Change Initiative (ESA CCI) soil moisture dataset, which is derived from multiple active microwave scatterometers and passive microwave radiometers to provide a temporally consistent and global daily soil moisture record[28]. The complete Version 09.2 record covers the period from 1978 to 2024. In this study, ESA CCI soil moisture was used to identify flash droughts and characterize their onset because of its global coverage and daily temporal resolution[71–74]. In situ soil water content from FLUXNET2015 sites was used to independently assess the temporal variability of daily soil moisture. The FLUXNET dataset has 207 sites providing soil moisture; however, only a few sites have observational records spanning decades[75]. We therefore used all sites with valid soil water content measurements and compared the temporal variations in the station observations with those from the corresponding ESA CCI grid cells. Given the limited temporal continuity and spatial representativeness of the station observations, ESA CCI soil moisture was used for flash drought analyses. Daily evaporation and potential evaporation from GLEAM v4.2[76] and hourly meteorological variables from ERA5[77], including 2-m air temperature, 2-m dewpoint temperature, shortwave radiation and total cloud fraction, were also used to investigate the physical mechanisms driving flash drought onset.

To characterize the variability of aerosol changes during the flash drought onset stage, both AOD and flash drought onset speed were converted to standardized anomalies. For each variable $y(t)$, the standardized time series is defined as:

$$y_z(t) = \frac{y(t) - \bar{y}}{\sigma_y} \tag{1}$$

where $\bar{y}$ and σ_y are the mean and standard deviation of y calculated over global land from 2003 to 2024. This standardization was applied separately to AOD and onset speed, denoted as AOD_z and $Speed_z$ in Fig. 1, respectively. For the regional and global scale analyses, grid-level AOD and onset speed were first spatially averaged using area weights and then standardized.

CMIP6 climate model simulations

We obtained daily soil moisture from the Coupled Model Intercomparison Project Phase 6 (CMIP6) model simulations to characterize flash droughts across global land areas, utilizing outputs from multiple Earth System Models to enhance the robustness of the simulations and reduce uncertainty (Supplementary Table S2)[29]. To isolate the contributions of individual external forcings to flash drought characteristics, we analyzed simulations from the Detection and Attribution Model Intercomparison Project (DAMIP), a coordinated framework within CMIP6 that includes three key forcing components: anthropogenic greenhouse gas concentrations (GHG), anthropogenic aerosol emissions (AER), and natural forcings including solar irradiance variations and volcanic aerosol loading (NAT)[30]. For future projections, we examined the period 2015–2100 under the Shared Socioeconomic Pathway 2-Representative Concentration Pathway 4.5 (SSP2-4.5) scenario, which represents a moderate mitigation pathway with intermediate greenhouse gas emissions and socioeconomic development, and analyzed three additional SSP2-4.5 single-forcing experiments (SSP2-4.5-GHG, SSP2-4.5-AER, and SSP2-4.5-NAT) to assess the relative importance of different forcing mechanisms in the future climate[78]. All model outputs were processed from native model resolutions to a uniform $1° \times 1°$ latitude-longitude grid using bilinear interpolation following established CMIP6 data processing procedures, and the analysis encompassed all terrestrial grid cells, providing a global assessment of external forcing impacts.

Flash drought identification and characterization

We first aggregated surface soil moisture to a pentad scale (5-day interval), such as January 1–5, at each grid cell. The pentad soil moisture was then converted to percentile rankings based on the temporal distribution of soil moisture for the corresponding pentad during the baseline period for each grid cell. In this study, the identification methodology employs three stringent criteria, emphasizing rapid development: (1) Soil moisture must decline from above the 40th percentile to below the 20th percentile, representing a transition from near-normal to severely dry conditions; (2) A minimum total duration must exceed 3 pentads (15 days) to distinguish flash drought events from short-term variability; (3) The decline rate of soil moisture must exceed the 5th percentile of decline rates, ensuring only the most rapidly developing events are classified as flash droughts. Flash drought termination was defined by the recovery of soil moisture above the 20th percentile. The onset period was defined as the duration required to satisfy criterion (1), and the onset speed was quantified by the rate of decrease in soil moisture percentile from above the 40th percentile to below the 20th percentile during each event. This framework ensures consistent reference across all reanalysis products and climate model simulations, enabling comparative analysis of flash drought development under different anthropogenic forcing scenarios.

The detection of flash drought episodes is sensitive to the choice of products, parameters, and analytical methodologies employed. The aforementioned criteria utilized in this study have been applied extensively in existing studies[1,3,79]. To enhance reliability and consistency, we employed several complementary strategies. First, we adopted an ensemble methodology incorporating multiple soil moisture products for flash drought detection. Although individual products exhibit some variability, ensemble averaging reveals robust large-scale patterns. We used 11–37 ensemble members from each CMIP6 climate experiment for the multi-model ensemble, and the resulting climatology of flash drought closely aligns with that derived from observations. We also evaluated methodological sensitivity by varying the thresholds used to define soil moisture decline rates. This validation framework, combining multi-ensemble detection and threshold sensitivity analysis, improves the robustness of flash drought identification and strengthens confidence in the attribution of anthropogenic influences on flash drought acceleration.

Bivariate dependence using copulas and probability multiplication factor

To characterize the complex dependence between AOD and soil moisture decline, we employed bivariate copula functions to model their joint probability distribution. This copula-based approach provides a framework for analyzing concurrent extreme events and quantifying their joint occurrence[80]. The joint cumulative distribution function of two variables, X and Y, can be expressed as[81]:

$$F_{X,Y}(x,y) = P(X \le x,\ Y \le y) \tag{2}$$

where X and Y represent soil moisture and AOD during the flash drought onset period, respectively, and P denotes their joint probability distribution. The corresponding marginal distributions are defined as $F_X(x) = P(X \le x)$ and $F_Y(y) = P(Y \le y)$ for variables X and Y, respectively. According to Sklar's theorem, the joint distribution can be uniquely decomposed as:

$$F_{X,Y}(x,y) = C\left[F_X(x), F_Y(y)\right] = C(u,\ v),\ 0 \le u,\ v \le 1 \tag{3}$$

The fundamental transformation converts the marginal distributions $F_X(x)$ and $F_Y(y)$ into uniformly distributed variables u and v on the unit interval [0, 1], while the copula function C captures the complete dependence structure between the variables. To determine the

optimal copula family for our analysis, we evaluated multiple copula families, including the Gaussian, Student's t, Clayton, Gumbel, and Frank copulas, each designed to capture distinct dependence patterns[81]. Model selection was performed using the Bayesian Information Criterion (BIC) to identify the most appropriate copula representation for each grid cell.

We quantified the concurrent probabilities of soil moisture and AOD deficits at multiple threshold levels. Specifically, we calculated the joint occurrence probability of soil moisture below the 30th percentile and AOD below the 30th percentile as $P(u<0.3\cap v<0.3)$. To assess increasingly severe drought conditions, we further evaluated joint probabilities for more extreme thresholds: $P(u<0.2\cap v<0.3)$, $P(u<0.1\cap v<0.3)$ and $P(u<0.05\cap v<0.3)$. Additionally, we applied the probability multiplication factor (PMF) to quantify how the dependence between soil moisture declines and AOD varies. The PMF is defined as the ratio of joint probability to the product of marginal probabilities, where a PMF value greater than 1 indicates positive dependence that amplifies the likelihood of concurrent extreme events.

Dynamic impacts of aerosol on flash drought onset speed

Traditional linear regression with constant coefficients cannot adequately capture the non-stationary influences of predictors on response variables. However, the relationship between atmospheric aerosols and soil moisture is non-stationary in a changing climate system. For instance, the cooling effects of aerosols have declined over the recent two decades[12,82]. Recent studies have demonstrated that aerosols exert varying impacts on hydrometeorological variables and extreme events[14,22,83]. To address these temporal dynamics, we employed a Bayesian Dynamic Linear Model (DLM) to examine the evolving relationships between aerosols and flash drought onset speed. The Bayesian DLM overcomes this limitation by allowing regression coefficients (b_i) to vary temporally[36,84,85]. This capability enables characterization of time-evolving influences exerted by predictor variables X_i on the response variable Y:

$$Y(t)=b_0(t)+b_1(t)X_1(t)+\cdots+b_M(t)X_M(t)+\varepsilon(t) \tag{4}$$

$$b_i(t)=b_i(t-1)+w_i(t) \tag{5}$$

where $\varepsilon(t)\sim N[0,V(t)]$ and $w_i(t)\sim N\left[0,W_i(t)\right]$ are independent noise terms, distributed normally with a mean of 0 and variances of $V(t)$ and $W_i(t)$.

The state equation (Eq. (5)) describes the evolution of the parameters at each step based on the previous state and current observations. Bayes' theorem integrates prior information with observations to sequentially update parameter distributions. We employed a Bayesian DLM to investigate the non-stationary impacts of aerosols on the onset speed of flash drought. Flash drought onset speed is jointly regulated by multiple factors, such as surface temperature (T2M), shortwave radiation (SWR), precipitation, VPD, soil moisture (SM), vertically integrated moisture divergence (VIMD), and 850hPa vertical velocity (w). Thus, we incorporated these factors into the model simulations to account for their confounding effects and to more robustly quantify the independent contribution of the processed AOD-related variable. Before performing the Bayesian DLM, we examined the multicollinearity among candidate variables using a backward-elimination procedure, whereby variables exceeding a VIF threshold of 5 in more than half of all regions were iteratively removed. Then, the effects of confounding factors on AOD were also removed:

$$AOD=a_0+\sum a_k x_k+\varepsilon \tag{6}$$

$$AOD_{residual}=AOD-\left(a_0+\sum a_k x_k\right) \tag{7}$$

In this study, X_1-X_M represent $AOD_{residual}$, T2M, SWR, SM, VIMD, and w, respectively, and $Y(t)$ represents the onset speed of flash drought. This multivariate framework reduces the likelihood that the inferred AOD effect merely reflects covarying climate variability rather than an independent aerosol-related influence. The $b_0(t)$ term represents a time-varying level or intercept whose variability is unexplained by the independent predictors X_1-X_M, while the b_1 term represents the non-stationary influence of X_1 on Y. A 10-yr moving window is used to investigate the temporal evolution of the impacts of AOD on onset speed by comparing the contribution of AOD in Bayesian DLM simulations and observed $Y(t)$. This temporal approach helps to capture the changing relationship between human-induced aerosol emissions and flash drought onset speed.

Structural equation modeling

We employed structural equation modeling (SEM) analysis to estimate pathway relationships among aerosol-induced climate changes during the onset stage of flash drought. The analysis was conducted using the Lavaan package[86], which applied covariance structure modeling to decompose multivariate associations by reconstructing the observed variance-covariance matrix. The model performance was evaluated using a chi-squared test that compares the estimated and the observed covariance matrices. Acceptable model fit ($P>0.05$) suggests that the proposed path adequately captures the underlying structure. We assessed the model using additional fit indices, including the Comparative Fit Index, Goodness-of-Fit Index, and Standardized Root Mean Square Residual.

Our conceptual framework synthesized established climatological relationships from previous research[1,5]. Aerosols, acting as the primary driver, influence multiple climatic variables, including total cloud cover, air temperature, and shortwave radiation. The framework conceptualizes flash drought onset speed as responding to interconnected factors of soil moisture declines and evaporation. We hypothesized that aerosol-induced changes in cloud cover and temperature modulate soil moisture and evaporation, which further lead to changes in flash drought onset speed. On the other hand, aerosols influence evaporation by modifying shortwave radiation. Given documented evidence linking climatic variables to soil drying processes, we also compared potential evapotranspiration and vapor pressure deficit as pathways in our analyses. The multi-factor approach acknowledges that flash drought onset results from complex interactions among water availability, atmospheric demand and radiation, modulated by aerosol changes.

Risk ratio assessment of anthropogenic impacts

We analyzed the global and regional risks of accelerated flash drought onset speed by employing probability ratios (PR). The PR metric, also termed the risk ratio, provides a quantification of flash drought acceleration risk attributable to human-induced climate changes relative to natural forcing alone[87,88]. The PR for each grid is defined as:

$$PR=\frac{P_{AC}}{P_{NAT}} \tag{8}$$

where P_{AC} represents the probability of flash drought onset speed simulated by individual anthropogenic forcings, including P_{AA} (AA-only) and P_{GHG} (GHG-only) forcings. P_{NAT} represents the probability of flash drought onset speed from NAT-only forcing. The risk ratio is calculated at each land grid cell. In this study, we focused on the assessment of the risk ratio associated with anthropogenic aerosols during the historical (1990–2019) and future periods (2030–2099).

Reporting summary

Further information on research design is available in the Nature Portfolio Reporting Summary linked to this article.

Data availability

Daily MODIS Collection 6.1 Level 3 data (MOD08_D3 and MYD08_D3) are available at https://ladsweb.modaps.eosdis.nasa.gov/. Daily AOD observations are available at https://aeronet.gsfc.nasa.gov/new_web/aerosols.html. Daily soil moisture from the European Space Agency Climate Change Initiative is available at https://climate.esa.int/en/data/. Soil moisture from the FLUXNET community is available at https://fluxnet.org/data/download-historical-data/. Potential evaporation is available at https://www.gleam.eu/. Atmospheric variables from ERA5 are available at https://cds.climate.copernicus.eu/datasets. The CMIP6 climate model simulations and individual anthropogenic forcing experiments from DAMIP are available through the Earth System Grid Federation at https://esgf-node.llnl.gov/search/cmip6/.

Code availability

The code used for analysis is available at https://doi.org/10.5281/zenodo.22977310.

References

1. Qing, Y. et al. Accelerating flash droughts induced by the joint influence of soil moisture depletion and atmospheric aridity. *Nat. Commun.* **13**, 1139 (2022).
2. Pendergrass, A. G. et al. Flash droughts present a new challenge for subseasonal-to-seasonal prediction. *Nat. Clim. Change* **10**, 191–199 (2020).
3. Yuan, X. et al. A global transition to flash droughts under climate change. *Science* **380**, 187–191 (2023).
4. Christian, J. I. et al. Global distribution, trends, and drivers of flash drought occurrence. *Nat. Commun.* **12**, 6330 (2021).
5. Zeng, Z. et al. Increased risk of flash droughts with raised concurrent hot and dry extremes under global warming. *npj Clim. Atmos. Sci.* **6**, 134 (2023).
6. Otkin, J. A. et al. Assessing the evolution of soil moisture and vegetation conditions during the 2012 United States flash drought. *Agric. For. Meteorol.* **218–219**, 230–242 (2016).
7. Jing, Y. et al. Gross primary productivity is more sensitive to accelerated flash droughts. *Commun. Earth Environ.* **6**, 34 (2025).
8. Yuan, X. et al. Anthropogenic shift towards a higher risk of flash drought over China. *Nat. Commun.* **10**, 4661 (2019).
9. Otkin, J. A. et al. Getting ahead of flash drought: from early warning to early action. *Bull. Am. Meteorol. Soc.* **103**, E2188–E2202 (2022).
10. AghaKouchak, A. et al. Toward impact-based monitoring of drought and its cascading hazards. *Nat. Rev. Earth Environ.* **4**, 582–595 (2023).
11. Gerken, T. et al. Convective suppression before and during the United States Northern Great Plains flash drought of 2017. *Hydrol. Earth Syst. Sci.* **22**, 4155–4163 (2018).
12. Quaas, J. et al. Robust evidence for reversal of the trend in aerosol effective climate forcing. *Atmos. Chem. Phys.* **22**, 12221–12239 (2022).
13. Samset, B. H. et al. Climate impacts from the removal of anthropogenic aerosol emissions. *Geophys. Res. Lett.* **45**, 1020–1029 (2018).
14. Wang, P. et al. Aerosols overtake greenhouse gases, causing a warmer climate and more weather extremes toward carbon neutrality. *Nat. Commun.* **14**, 7257 (2023).
15. Bellouin, N. et al. Bounding global aerosol radiative forcing of climate change. *Rev. Geophys.* **58**, e2019RG000660 (2020).
16. Li, J. et al. Scattering and absorbing aerosols in the climate system. *Nat. Rev. Earth Environ.* **3**, 363–379 (2022).
17. Seinfeld, J. H. et al. Improving our fundamental understanding of the role of aerosol–cloud interactions in the climate system. *Proc. Natl. Acad. Sci. USA* **113**, 5781–5790 (2016).
18. Gryspeerdt, E. et al. Uncertainty in aerosol–cloud radiative forcing is driven by clean conditions. *Atmos. Chem. Phys.* **23**, 4115–4122 (2023).
19. Miralles, D. G. et al. Land–atmospheric feedbacks during droughts and heatwaves: state of the science and current challenges. *Ann. N.Y. Acad. Sci.* **1436**, 19–35 (2019).
20. Feichter, J. et al. Nonlinear Aspects of the Climate Response to Greenhouse Gas and Aerosol Forcing. *J. Clim.* **17**, 2384–2398 (2004).
21. Chang, I. et al. Spatiotemporal heterogeneity of aerosol and cloud properties over the southeast Atlantic: An observational analysis. *Geophys. Res. Lett.* **48**, e2020GL091469 (2021).
22. Wei, J. et al. Reduced anthropogenic aerosols reveal increased heatwaves driven by climate warming. *Earth's Future* **13**, e2025EF006516 (2025).
23. Chiang, F., Mazdiyasni, O. & AghaKouchak, A. Evidence of anthropogenic impacts on global drought frequency, duration, and intensity. *Nat. Commun.* **12**, 2754 (2021).
24. Kuo, Y. N. et al. Recent southwestern US drought was exacerbated by anthropogenic aerosols and tropical ocean warming. *Nat. Geosci.* **18**, 578–585 (2025).
25. Platnick, S., King, M., Hubanks, P. MODIS Atmosphere L3 Daily Product. NASA MODIS Adaptive Processing System, Goddard Space Flight Center https://doi.org/10.5067/MODIS/MOD08_D3.061 (2017).
26. Giles, D. M. et al. Advancements in the Aerosol Robotic Network (AERONET) version 3 database–automated near-real-time quality control algorithm with improved cloud screening for Sun photometer aerosol optical depth (AOD) measurements. *Atmos. Meas. Tech.* **12**, 169–209 (2019).
27. Holben, B. N. et al. AERONET—A federated instrument network and data archive for aerosol characterization. *Remote Sens. Environ.* **66**, 1–16 (1998).
28. Dorigo, W. A. et al. ESA CCI Soil Moisture for improved Earth system understanding: State-of-the-art and future directions. *Remote Sens. Environ.* **203**, 185–215 (2017).
29. Eyring, V. et al. Overview of the Coupled Model Intercomparison Project Phase 6 (CMIP6) experimental design and organization. *Geosci. Model. Dev.* **9**, 1937–1958 (2016).
30. Gillett, N. P. et al. The Detection and Attribution Model Intercomparison Project (DAMIP v1.0) contribution to CMIP6. *Geosci. Model. Dev.* **9**, 3685–3697 (2016).
31. Christian, J. I. et al. Global projections of flash drought show increased risk in a warming climate. *Commun. Earth Environ.* **4**, 165 (2023).
32. Bollasina, M. A., Ming, Y. & Ramaswamy, V. Anthropogenic aerosols and the weakening of the South Asian summer monsoon. *Science* **334**, 502–505 (2011).
33. Zhou, S. et al. Land–atmosphere feedbacks exacerbate concurrent soil drought and atmospheric aridity. *Proc. Natl. Acad. Sci. USA* **116**, 18848–18853 (2019).
34. Ullah, I. et al. Anthropogenic and atmospheric variability intensify flash drought episodes in South Asia. *Commun. Earth Environ.* **5**, 267 (2024).
35. Han, W. et al. Sea level extremes and compounding marine heatwaves in coastal Indonesia. *Nat. Commun.* **13**, 6410 (2022).
36. Wei, J. et al. Intensification of heatwaves in China in recent decades: roles of climate modes. *npj Clim. Atmos. Sci.* **6**, 98 (2023).
37. Hermant, A., Huusko, L. & Mauritsen, T. Increasing aerosol direct effect despite declining global emissions in MPI-ESM1.2. *Atmos. Chem. Phys.* **24**, 10707–10715 (2024).
38. Ramanathan, V. et al. Aerosols, climate, and the hydrological cycle. *Science* **294**, 2119–2124 (2001).
39. Kaufman, Y. J., Tanré, D. & Boucher, O. A satellite view of aerosols in the climate system. *Nature* **419**, 215–223 (2002).
40. Andreae, M. O., Jones, C. D. & Cox, P. M. Strong present-day aerosol cooling implies a hot future. *Nature* **435**, 1187–1190 (2005).

41. Yu, H. et al. A review of measurement-based assessments of the aerosol direct radiative effect and forcing. *Atmos. Chem. Phys.* **6**, 613–666 (2006).
42. IPCC. Climate Change. 2022: Mitigation of Climate Change. *Contribution of Working Group III to the Sixth Assessment Report of the Intergovernmental Panel on Climate Change* (Cambridge University Press, 2022).
43. Diffenbaugh, N. S. & Barnes, E. A. Data-driven predictions of the time remaining until critical global warming thresholds are reached. *Proc. Natl. Acad. Sci. USA* **120**, e2207183120 (2023).
44. Sayer, A. M. et al. Validation, stability, and consistency of MODIS collection 6.1 and VIIRS version 1 deep blue aerosol data over land. *J. Geophys. Res. Atmos.* **124**, 4658–4688 (2019).
45. Zhang, J. & Reid, J. S. An analysis of clear sky and contextual biases using an operational over ocean MODIS aerosol product. *Geophys. Res. Lett.* **36**, L15824 (2009).
46. Schutgens, N. et al. On the spatio-temporal representativeness of observations. *Atmos. Chem. Phys.* **17**, 9761–9780 (2017).
47. Lawrence, D. M. et al. The Community Land Model version 5: description of new features, benchmarking, and impact of forcing uncertainty. *J. Adv. Model. Earth Syst.* **11**, 4245–4287 (2019).
48. Walters, D. et al. The Met Office Unified Model Global Atmosphere 7.0/7.1 and JULES Global Land 7.0 configurations. *Geosci. Model Dev.* **12**, 1909–1963 (2019).
49. Boucher, O. et al. Presentation and evaluation of the IPSL-CM6A-LR climate model. *J. Adv. Model. Earth Syst.* **12**, e2019MS002010 (2020).
50. Voldoire, A. et al. Evaluation of CNRM climate models for CMIP6. *J. Adv. Model. Earth Syst.* **11**, 4182–4227 (2019).
51. Swart, N. C. et al. The Canadian Earth System Model version 5 (CanESM5.0.3). *Geosci. Model Dev.* **12**, 4823–4873 (2019).
52. Ziehn, T. et al. The Australian Earth System Model: ACCESS-ESM1.5. *J. Adv. Model. Earth Syst.* **12**, e2020MS002121 (2020).
53. Wu, T. et al. The Beijing Climate Center Climate System Model (BCC-CSM): the main progress from CMIP5 to CMIP6. *Geosci. Model Dev.* **12**, 1573–1600 (2019).
54. Yukimoto, S. et al. The Meteorological Research Institute Earth System Model Version 2.0, MRI-ESM2.0: description and basic evaluation of the physical component. *J. Meteorol. Soc. Jpn.* **97**, 931–965 (2019).
55. Jessen, S. et al. Hydrology and pore water chemistry in a permafrost wetland, Ilulissat, Greenland. *Water Resour. Res.* **50**, 4760–4774 (2014).
56. Maryol, E. & Lin, C. Geochemical characteristics of soils in Fezzan, Sahara Desert: Implications for environment and agriculture. *J. Geochem. Explor.* **158**, 122–131 (2015).
57. Kopacz, M. et al. Origin and radiative forcing of black carbon transported to the Himalayas and Tibetan Plateau. *Atmos. Chem. Phys.* **11**, 2837–2852 (2011).
58. Han, H. et al. Impacts of atmospheric transport and biomass burning on the inter-annual variation in black carbon aerosols over the Tibetan Plateau. *Atmos. Chem. Phys.* **20**, 13591–13610 (2020).
59. Hu, Z. et al. Modeling dust sources, transport, and radiative effects at different altitudes over the Tibetan Plateau. *Atmos. Chem. Phys.* **20**, 1507–1529 (2020).
60. Aouizerats, B. et al. Importance of transboundary transport of biomass burning emissions to regional air quality in Southeast Asia during a high fire event. *Atmos. Chem. Phys.* **15**, 363–373 (2015).
61. Ginoux, P. et al. Global-scale attribution of anthropogenic and natural dust sources and their emission rates based on MODIS Deep Blue aerosol products. *Rev. Geophys.* **50**, RG3005 (2012).
62. Ding, K. et al. Aerosol-boundary-layer-monsoon interactions amplify the semi-direct effect of biomass smoke on low cloud formation in Southeast Asia. *Nat. Commun.* **12**, 6416 (2021).
63. Sarkar, A. et al. Influence of smoke aerosols on low-level clouds over the Indian region during winter. *Atmos. Res.* **278**, 106358 (2022).
64. Berg, A. et al. Land–atmosphere feedbacks amplify aridity increase over land under global warming. *Nature Clim. Change* **6**, 869–874 (2016).
65. Seneviratne, S. I. et al. Investigating soil moisture–climate interactions in a changing climate: A review. *Earth-Sci. Rev.* **99**, 125–161 (2010).
66. Wang, F. et al. Arctic amplification-induced decline in West and South Asia dust warrants stronger anti-desertification efforts toward carbon neutrality. *Proc. Natl. Acad. Sci. USA.* **121**, e2317444121 (2024).
67. Wang, L. et al. Recent accelerated drying in southwest China is dominated by anthropogenic aerosol forcing. *Environ. Res. Lett.* **21**, 014035 (2026).
68. Jiang, J. & Zhou, T. A strengthened and southward-shifted westerly jet mitigates warming-induced drying across Asian drylands. *Sci. Adv.* **12**, eaed7890 (2026).
69. Hsu, N. C. et al. Enhanced Deep Blue aerosol retrieval algorithm: the second generation. *J. Geophys. Res. Atmos.* **118**, 9296–9315 (2013).
70. Sayer, A. M. et al. MODIS Collection 6 aerosol products: comparison between Aqua's e-Deep Blue, Dark Target, and "merged" data sets, and usage recommendations. *J. Geophys. Res. Atmos.* **119**, 13,965–13,989 (2014).
71. Gruber, A. et al. Evolution of the ESA CCI Soil Moisture Climate Data Records and their underlying merging methodology. *Earth Syst. Sci. Data* **11**, 717–739 (2019).
72. Gruber, A. et al. Triple collocation-based merging of satellite soil moisture retrievals. *IEEE Trans. Geosci. Remote Sens.* **55**, 6780–6792 (2017).
73. Liu, Y. Y. et al. Developing an improved soil moisture dataset by blending passive and active microwave satellite-based retrievals. *Hydrol. Earth Syst. Sci.* **15**, 425–436 (2011).
74. Preimesberger, W., et al. Homogenization of Structural Breaks in the Global ESA CCI Soil Moisture Multisatellite Climate Data Record, in *IEEE Trans. Geosci. Remote Sens*. 59, pp 2845–286 (2021).
75. Pastorello, G. et al. The FLUXNET2015 dataset and the ONEFlux processing pipeline for eddy covariance data. *Sci. Data* **7**, 225 (2020).
76. Miralles, D. G. et al. GLEAM4: global land evaporation and soil moisture dataset at 0.1° resolution from 1980 to the present. *Sci. Data* **12**, 416 (2025).
77. Hersbach, H. et al. The ERA5 global reanalysis. *Q. J. R. Meteorol. Soc.* **146**, 1999–2049 (2020).
78. O'Neill, B. C. et al. The Scenario Model Intercomparison Project (ScenarioMIP) for CMIP6. *Geosci. Model. Dev.* **9**, 3461–3482 (2016).
79. Sehgal, V., Gaur, N. & Mohanty, B. P. Global flash drought monitoring using surface soil moisture. *Water Resour. Res.* **57**, e2020WR029901 (2021).
80. Zscheischler, J. et al. A typology of compound weather and climate events. *Nat. Rev. Earth Environ.* **1**, 333–347 (2020).
81. Salvadori, G. & De Michele, C. Frequency analysis via copulas: theoretical aspects and applications to hydrological events. *Water Resour. Res.* **40**, W12511 (2004).
82. Samset, B. H. et al. East Asian aerosol cleanup has likely contributed to the recent acceleration in global warming. *Commun. Earth Environ.* **6**, 543 (2025).
83. Persad, G. G. & Caldeira, K. Divergent global-scale temperature effects from identical aerosols emitted in different regions. *Nat. Commun.* **9**, 3289 (2018).
84. Petris, G., Petrone, S. & Campagnoli, P. *Dynamic Linear Models with R* (Springer, 2009).

85. Han, W. et al. Decadal variability of the Indian and Pacific Walker cells since the 1960s: Do they covary on decadal time scales? *J. Clim.* **30**, 8447–8468 (2017).
86. Rosseel, Y. Lavaan: an R package for structural equation modeling. *J. Stat. Softw.* **48**, 1–36 (2012).
87. Stott, P. A., Stone, D. A. & Allen, M. R. Human contribution to the European heatwave of 2003. *Nature* **432**, 610–614 (2004).
88. Thiery, W. et al. Warming of hot extremes alleviated by expanding irrigation. *Nat. Commun.* **11**, 290 (2020).

Acknowledgments

We thank the State Key Laboratory of Climate Resilience for Coastal Cities and the Department of Land Surveying and Geospatial Science of the Hong Kong Polytechnic University, the College of Hydrology and Water Resources of Hohai University, and the Society of Hong Kong Scholars for their support of this research.

Author contributions

J.W. and S.W. conceived and designed the study. J.W. processed the data, conducted the analysis, and drafted the manuscript. S.W. supervised the study. W.W., J.A.O., D.G.M., and A.A. provided valuable comments for improving the quality of the manuscript. All authors contributed to the interpretation and discussion of the results and revised the manuscript.

Funding

This work was supported by grants from the Research Grants Council of the Hong Kong Special Administrative Region, China (project no. PolyU/RGC 15232023) and the Hong Kong Polytechnic University (project no. P0052737). J.W. is supported by the National Natural Science Foundation of China (42307117) and the Hong Kong Scholars Program (XJ2024046). D.G.M. acknowledges the support received from the European Research Council under grant agreement number 101088405 (HEAT).

Competing interests

The authors declare no competing interests.

Additional information

Supplementary information The online version contains supplementary material available at https://doi.org/10.1038/s41467-026-78230-4.

Correspondence and requests for materials should be addressed to Shuo Wang.

Peer review information *Nature Communications* thanks Emily Black and the other anonymous reviewer(s) for their contribution to the peer review of this work. A peer review file is available.

Reprints and permissions information is available at http://www.nature.com/reprints

Publisher's note Springer Nature remains neutral with regard to jurisdictional claims in published maps and institutional affiliations.

Open Access This article is licensed under a Creative Commons Attribution-NonCommercial-NoDerivatives 4.0 International License, which permits any non-commercial use, sharing, distribution and reproduction in any medium or format, as long as you give appropriate credit to the original author(s) and the source, provide a link to the Creative Commons licence, and indicate if you modified the licensed material. You do not have permission under this licence to share adapted material derived from this article or parts of it. The images or other third party material in this article are included in the article's Creative Commons licence, unless indicated otherwise in a credit line to the material. If material is not included in the article's Creative Commons licence and your intended use is not permitted by statutory regulation or exceeds the permitted use, you will need to obtain permission directly from the copyright holder. To view a copy of this licence, visit http://creativecommons.org/licenses/by-nc-nd/4.0/.

© The Author(s) 2026